Strongly Coupled Single-Quantum-Dot–Cavity System Integrated on a CMOS-Processed Silicon Photonic Chip

A. Osada,[1,*] Y. Ota,[1] R. Katsumi,[2] M. Kakuda,[1] S. Iwamoto,[1,2] and Y. Arakawa[1]

[1] *Institute for Nano Quantum Information Electronics, The University of Tokyo, Meguro-ku, Tokyo 153-8505, Japan*

[2] *Institute of Industrial Science, The University of Tokyo, Meguro-ku, Tokyo 153-8505, Japan*

(Received 28 September 2018; revised manuscript received 18 December 2018; published 27 February 2019)

A quantum photonic integrated circuit (QPIC) is a promising tool for constructing integrated devices for quantum-technology applications. In the optical regime, silicon photonics empowered by complementary-metal-oxide-semiconductor (CMOS) technology provides optical components useful for realizing large-scale QPICs. Optical nonlinearity at the single-photon level is required for QPICs to facilitate photon-photon interaction. However, to date, realization of optical elements with deterministic (i.e., not probabilistic) single-photon nonlinearity by use of silicon-based components is challenging despite the enhancement of the functionality of QPICs based on silicon photonics. In this study, we realize a strongly coupled InAs/GaAs quantum-dot–cavity-quantum-electrodynamics system on a CMOS-processed silicon photonic chip. The heterogeneous integration of the GaAs cavity on the silicon chip is performed by transfer printing. The cavity-quantum-electrodynamics system on the CMOS photonic chip realized in this work is a promising candidate for an on-chip single-photon nonlinear element, which constitutes the fundamental component for future applications based on QPICs, such as coherent manipulation and nondestructive measurement of qubit states via a cavity, and an efficient single-photon filter and router.

DOI: 10.1103/PhysRevApplied.11.024071

I. INTRODUCTION

Quantum photonic integrated circuits (QPICs) [1,2], comprising various quantum optical elements assembled on a single chip, are intensively studied as promising tools for the implementation of quantum devices for quantum-technology applications [3–6]. Various elements commonly used for quantum- and classical-optics devices, such as beam splitters and modulators, are well developed on the basis of a silicon-photonics platform [7,8], which uses the complementary-metal-oxide-semiconductor (CMOS) process. However, in silicon photonics, elements with single-photon nonlinearity have not been implemented despite their ability to realize photon-photon interaction required for applications such as universal quantum computation. As a candidate for realizing such elements, a system involving an optical cavity with a single two-level emitter, which is called the "cavity-quantum-electrodynamics (cavity-QED) system," is of significant interest. The cavity-QED system has been investigated with various two-level emitters [9–16]. Strong modification of the electromagnetic environment surrounding the emitter by use of cavities and waveguides has allowed researchers to achieve various quantum optical elements (e.g., efficient and fast single-photon sources [17–20], single-photon switches and routers [21–23], and Fock-state filters [24,25]).

Among the cavity-QED systems, the one with a semiconductor quantum dot (QD) is promising for integration into QPICs because of its well-developed electrical controllability and availability of telecommunication-compatible emission wavelengths that might be suitable for silicon photonics. Some heterogeneously integrated QD light sources without optical cavities [26–28] have been implemented by, for example, wafer bonding on silicon-based photonic circuits. However, cavity-QED-based elements combined with CMOS photonic circuitry are yet to be realized despite their considerable potential to provide highly functional single-photon devices to be integrated with QPICs. Even without the use of CMOS technology, only a limited number of realizations of cavity-QED systems on a Si platform [29,30] have been reported so far, where Davanco *et al.* [29] used a silicon nitride system and Luxmoore *et al.* [30] implemented cavity-QED systems on a hybrid substrate without any silicon-based photonic elements. The main obstacle here is the complicated process optimization required to simultaneously fabricate a nanoscale compound-semiconductor cavity and a low-loss silicon photonic element. This issue can be resolved by transfer printing [31–33], which allows

*alto@iis.u-tokyo.ac.jp

pick-and-place heterogeneous integration of individually fabricated elements. Since transfer printing uses the van der Waals force for adhesion, it works without the adhesion layer and regardless of the materials used. Such a method is suitable for integrating nanoscale cavity-QED systems into CMOS-processed silicon photonic circuits, and even a cavity-QED system in the strong coupling regime on a CMOS photonic chip is feasible, which is particularly significant not only in view of efficient, on-chip coherent manipulation and nondestructive read-out of QD states by use of the cavity [34,35] but also because of its scalability and functionality aided by CMOS technology.

In this article, we demonstrate a strongly coupled single-QD–photonic-crystal (PC)-cavity system integrated on a CMOS-processed silicon photonic circuit by the transfer-printing method. A one-dimensional (1D) PC cavity containing InAs/GaAs QDs is transfer-printed on top of a silicon waveguide on a silicon-on-insulator (SOI) chip that is fabricated in a CMOS-process foundry. The device is designed to offer near-unity coupling efficiency to the waveguide and a high quality factor of the cavity. Microphotoluminescence spectroscopy reveals the vacuum Rabi splitting between the QD and the cavity, which indicates that the QD-cavity coupled system is in the strong coupling regime. We further analyze the spectra to obtain the coupling strength as $g_0 = 69\ \mu$eV and observe the interchanged peak heights and linewidths between the upper and lower polaritons, which substantiate the strong coupling. From a grating outcoupler terminating the waveguide, we observe the vacuum Rabi splitting that confirms the waveguide coupling of the system.

II. DESIGN AND FABRICATION

The device fabricated and investigated in this study is a 1D PC cavity [36–39] coupled to a silicon-wire waveguide buried in silicon dioxide, where the cavity strongly couples to a single QD embedded in it. A schematic illustration of the device is shown in Fig. 1(a). The PC cavity is formed by a nanobeam with almost equidistantly aligned air holes, where the distances between the adjacent air holes are modulated in the central region containing ten air holes [39]. The ratio of the radius r of the holes to the lattice constant a is 0.26. The nanobeam has a thickness of 180 nm and a width of 471 nm. The distribution of the electric field in the y direction of the fundamental cavity mode is calculated by the finite-difference time-domain (FDTD) method, and is shown in Fig. 1(b). The unloaded quality factor is 6×10^6 and the mode volume is $0.56\,(\lambda/n)^3$, where $\lambda = 1.16\ \mu$m is the resonant wavelength and $n = 3.4$ is the refractive index of GaAs. Here the unloaded (loaded) quality factor refers to that of the cavity on a silicon dioxide layer in the absence (presence) of the waveguide coupling. Underlying this is a silicon-wire waveguide buried in a silicon dioxide layer. Its thickness and

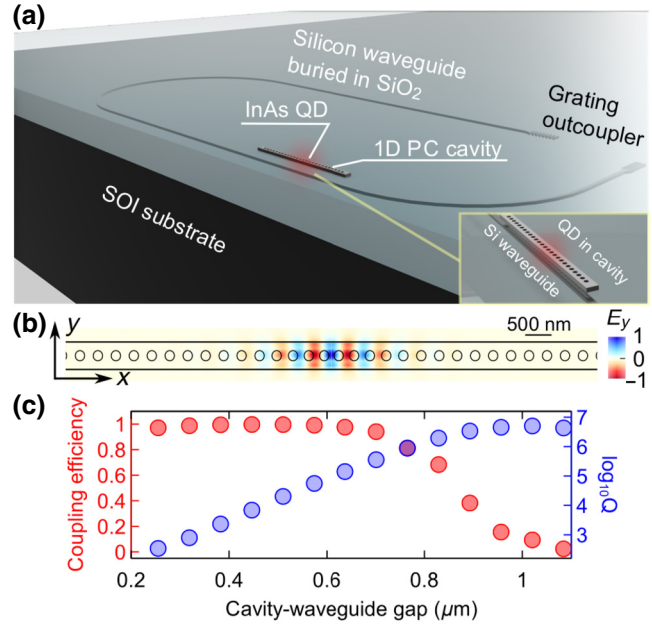

FIG. 1. (a) The device implementing a strongly coupled quantum-dot–cavity system integrated on a CMOS-processed silicon photonic circuit. (b) Calculated distribution of the y component of the electric field exhibited by the fundamental mode of the one-dimensional photonic crystal cavity. The field is normalized to the maximum value. (c) Numerically evaluated quality factor (blue, right axis) of the fundamental mode and the fraction of light coupled into the silicon waveguide (red, left axis) as a function of the distance between the cavity and the waveguide.

width are 210 and 250 nm, respectively, so the waveguide supports only a single transverse-electric mode at a wavelength of around 1160 nm. This also approximately fulfills the phase-matching condition between the waveguide and the cavity [40] for efficient coupling between them. The waveguide is terminated by grating outcouplers to collect the signal introduced to the waveguide from the cavity.

The cavity and the waveguide are separated by a silicon dioxide layer. The coupling efficiency (i.e., the ratio of light leaking from cavity mode into the silicon waveguide to total leakage) is controlled by the gap between the cavity and the waveguide in this design. As the cavity-waveguide gap becomes smaller, the loaded quality factor of the cavity mode decreases, while the coupling efficiency approaches unity [see the FDTD-calculation results in Fig. 1(c)]. The designed value of the gap, 570 nm, results in a coupling efficiency of 99% and a loaded quality factor of 4.8×10^4, which are advantageous together with the small mode volume of the cavity for the experiment conducted in this study. The high coupling efficiency in this design is attributed to the large unloaded quality factor of the cavity, as obtained in the numerical calculation.

The device is fabricated as follows. First, air-bridged 1D PCs supported by square frames are prepared by electron-beam lithography and dry and wet etching. The square

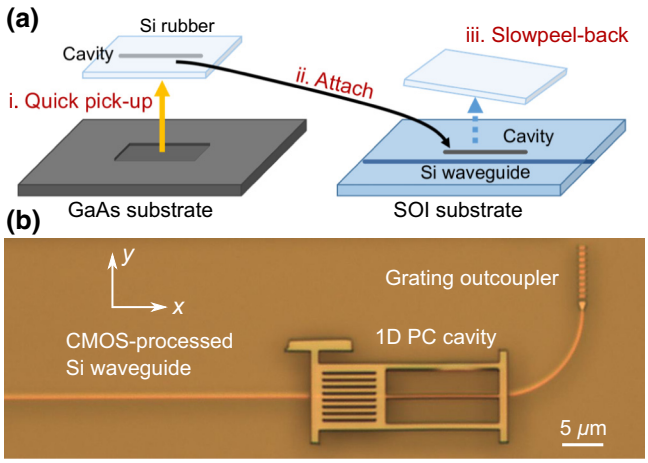

FIG. 2. (a) The transfer-printing process. An air-bridged one-dimensional photonic crystal cavity is picked up by silicone rubber from a GaAs chip and then attached to a silicon-on-insulator chip on top of a waveguide. By slow peeling back of the silicone rubber, the cavity is left on the waveguide. The whole procedure is monitored by an optical microscope. (b) Optical micrograph of the fabricated device, where a one-dimensional photonic crystal cavity is transfer-printed on a CMOS-processed silicon waveguide, which is terminated by grating outcouplers.

frame surrounding the PC cavity protects the cavity from bending and breaking and facilitates the picking-up process in transfer printing. The silicon-wire waveguides on a SOI substrate are fabricated in a CMOS-process foundry and are initially capped with a 1.8-μm-thick silicon dioxide layer formed by chemical-vapor deposition. The silicon dioxide layer on top of the silicon waveguides is thinned to 573 nm by dry etching. With these constituent elements, the device is fabricated by transfer printing, which is achieved by the picking up of a 1D PC cavity with silicon rubber, attachment of the cavity on top of the waveguide, and peeling back of the silicone rubber to leave the cavity on the SOI substrate. It has been shown that PC cavities can be transfer-printed with an alignment precision within 100 nm and with the quality factor maintained as high as approximately 10^4 [40,41]. These procedures are monitored with an optical microscope and are schematically illustrated in Fig. 2(a). An optical micrograph of the fabricated device is shown in Fig. 2(b), from which it is deduced that the alignment precision of the cavity with respect to the waveguide is less than 100 nm. Numerical calculation reveals that the waveguide coupling varies by a few percent within this alignment accuracy [40].

III. EXPERIMENTAL RESULTS

The fabricated device is evaluated by low-temperature microphotoluminescence spectroscopy with 785-nm wavelength; here the beam of a continuous-wave laser as a nonresonant excitation laser impinges on the cavity with an optical power of 9.8 μW through a $\times 50$ objective lens. First, we evaluate the device by collecting photoluminescence (PL) signals radiated above the cavity. Figure 3(a) displays the series of PL spectra for variable-wavelength detuning between the quantum dot (λ_{QD}) and the fundamental mode of the cavity (λ_{cav}). The wavelengths λ_{QD} and λ_{cav} are simultaneously tuned by our varying the temperature of the device from 10 to 35 K, where λ_{QD} varies more than λ_{cav}. In Fig. 3(a), the horizontal axis represents the wavelength of the QD relative to the resonant wavelength of the cavity, $\lambda_{cav} \sim 1155$ nm. The cavity mode exhibits a loaded quality factor of 8000, which corresponds to the total decay rate of the cavity, $\kappa_{tot} \sim 2\pi \times 32$ GHz, being larger than the linewidth of the QD, $\gamma_{QD} = 3$ GHz. These values are evaluated when $\lambda_{QD} - \lambda_{cav} = 0.5$ nm [see the top-left inset in Fig. 3(a)].

When $\lambda_{QD} = \lambda_{cav}$, an avoided crossing between the QD and the cavity is observed. The white curves in Fig. 3(a) indicate the positions of the peaks of upper and lower polaritons extracted by fitting, which also confirms the avoided-crossing behavior. The bottom-right inset displays the polarization of the observed signal above the cavity when $\lambda_{QD} - \lambda_{cav} = 0.5$ nm; see Fig. 2(b) for the definition of the x and y directions. The y-polarized signature agrees with the characteristics of the polarization of the cavity; hence, it is verified that the observed signal originates from the emission above the cavity. The spectrum at $\lambda_{QD} = \lambda_{cav}$ is shown in Fig. 3(b) together with the result of fitting (solid yellow line) with three Voigt functions for the peaks of the upper polariton (blue), lower polariton (green), and residual signal of the cavity (black) originating from the nonresonant excitation of the system [42,43]. Although the residual signal of the cavity coming from excitons other than the strongly coupled QD exciton hinders the observation of only two separate peaks, the fitting ensures the presence of two polaritons split in the strong-coupling regime. The vacuum Rabi splitting is given by

$$2\hbar\sqrt{g_0^2 - \left(\frac{\kappa_{tot}}{4} - \frac{\gamma}{4}\right)^2}$$

by the Jaynes-Cummings model [44] and is extracted from the spectrum to be 122 μeV, from which the coupling strength between the QD and the cavity is determined as $g_0 = 69\ \mu\text{eV} = 2\pi \times 17$ GHz. For coupling strength g_0, decay rate of the cavity $\kappa_{tot} = 2\pi \times 32$ GHz, and decay rate of the QD $\gamma_{QD} \ll \kappa_{tot}$, the system exhibits $g_0 > \kappa_{tot}/4$ and $\gamma_{QD}/4$, which fulfills the condition of strong coupling. In Figs. 3(c) and 3(d), respectively, peak heights and linewidths of the upper (blue) and lower (green) polaritons are plotted against $\lambda_{QD} - \lambda_{cav}$, with the solid curves representing the results of analytical simulation based on the Jaynes-Cummings model with relevant experimental parameters as guides for the eye. Both plots indicate the

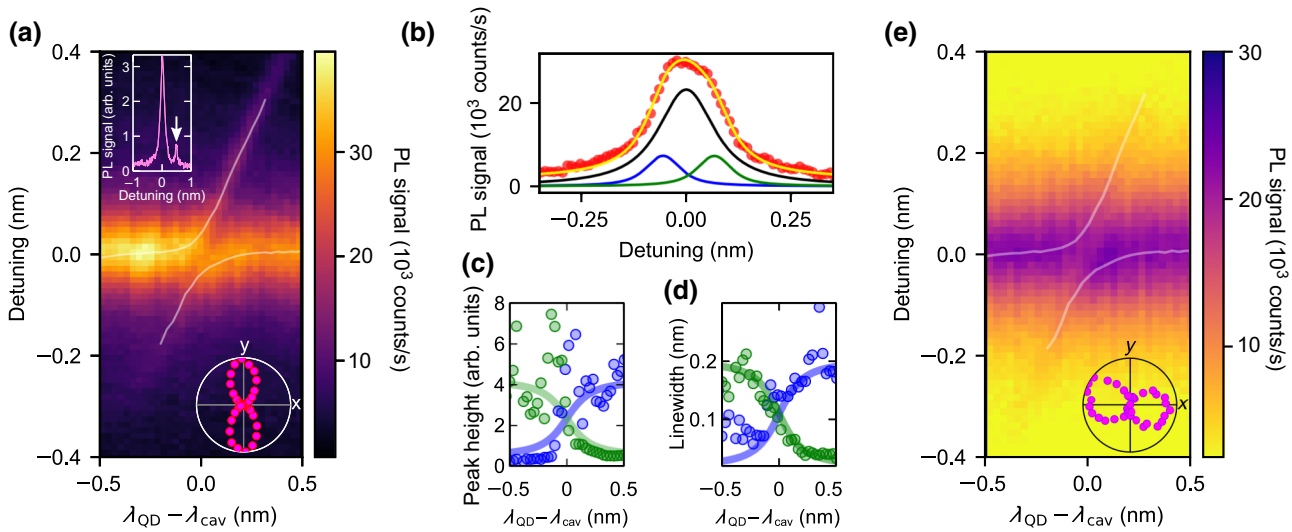

FIG. 3. (a) Color plot of PL spectra with the temperature of the device ranging from 10 to 35 K. The wavelength of the QD λ_{QD} relative to that of the cavity λ_{cav} is shown on the horizontal axis. The vertical axis represents the wavelength detuning from λ_{cav}. The white curves indicate the positions of peaks originating from the upper and lower polaritons extracted by fitting. A spectrum at $\lambda_{QD} - \lambda_{cav} = 0.5$ nm is displayed in the top-left inset, with the QD peak indicated by the white arrow. The polarization of the detected signal when $\lambda_{QD} - \lambda_{cav} = 0.5$ nm is shown in the bottom-right inset. (b) Spectrum at $\lambda_{QD} = \lambda_{cav}$ nm (red) analyzed by multipeak fitting (yellow) with the components of the upper (blue) and lower (green) polaritons and the bare cavity (black) plotted together. (c),(d) Extracted (c) peak heights and (d) linewidths of upper (blue) and lower (green) polaritons, with the solid curves indicating the simulated behavior. (e) Color plot of PL signals obtained from the grating outcoupler, plotted in the same way as in Fig. 3(a). The white curves indicate the positions of the upper and lower polaritons extracted in Fig. 3(a) as a guide for the eye. The polarization of the detected signal when $\lambda_{QD} - \lambda_{cav} = 0.5$ nm is shown in the inset.

interchanging spectral properties between the upper and lower polaritons over the avoided crossing, which further establishes the strong coupling between the QD and the cavity in this device.

Next the waveguide coupling of the cavity is examined by shining the excitation laser beam on the cavity and collecting the PL signal from the grating outcoupler. Here the irradiated optical power is 14 μW. The temperature of the device is again tuned from 10 to 35 K to obtain the spectrum shown in Fig. 3(e), which is plotted in the same way as Fig. 3(a), where the extracted positions of the upper and lower polaritons [i.e., the ones obtained in Fig. 3(a)] are shown again as guides for the eye. In the inset, the polarization of the observed signal when $\lambda_{QD} - \lambda_{cav} = 0.5$ nm is shown. The x-polarized light is expected to be radiated from the grating outcoupler, because the transverse-electric polarization of the light from the cavity coupled to the waveguide should be maintained. This is verified by the x-polarized nature of the signal. The avoided crossing is visible in the plot, ensuring the realization of the strongly coupled single-QD–cavity system accessible via the silicon waveguide on the CMOS platform. The signal of the QD is still observable when it is slightly off-resonant from the cavity; however, it is no longer visible as the QD-cavity detuning becomes larger, as the QD signal is expected to be visible only through the coupling to the cavity.

IV. DISCUSSION

Before summarizing the study, we briefly discuss the possible increase of the coupling strength between the QD and the cavity and the waveguide-coupling efficiency. First, the QD-cavity coupling strength depends significantly on the position of the QD within the cavity [45]. The coupling strength is expected to reach at least 93 μeV according to Ref. [39]. To integrate the QD-cavity system with larger coupling strength on a silicon photonic chip, the low yield, which is about several percent in this work, should be increased. The device yield is limited mainly by the uncertainty of the wavelength and position of the QD and the wavelength and quality factor of the cavity. The transfer-printing method permits back-end assembly after individual optimization and prescreening of the desired elements to address the aforementioned issues. This leads to deterministic integration of QD-cavity systems with larger coupling strength and quality factor of the cavity.

The waveguide-coupling efficiency can be estimated from the comparison of the loaded quality factor of the cavity with the unloaded quality factor. However, in the current case, the waveguide-coupling rate $\kappa_{WG} \sim 2\pi \times 5$ GHz determined by the FDTD calculation is small compared with the experimentally quantified total loss rate of the cavity, $\kappa_{tot} \sim 2\pi \times 32$ GHz, whose sample-to-sample

fluctuation hinders the relevant estimation of κ_{WG} in the experiment. By adopting the aforementioned values of κ_{WG} and κ_{tot}, we get the coupling efficiency $\eta_{exp} = \kappa_{WG}/\kappa_{tot} \sim$ 16%. The small value of η_{exp} not only hinders the relevant estimation of the coupling efficiency as mentioned above but also limits the signal-to-noise ratio of the spectrum in Fig. 3(e). If the unloaded quality factor of the cavity is increased to 8×10^4 [43] and the waveguide-coupling rate is increased to yield a loaded quality factor of 1×10^4, when we set the waveguide-resonator gap to be 450 nm the coupling efficiency becomes 88% while maintaining the system in the strong-coupling regime. These improvements pave the way to efficient optical control and dispersive read-out of the quantum states of a QD, and realization of single-photon nonlinear elements even enabling photon-number resolution, where the QPIC acquires further functionality and scalability on a CMOS-processed silicon photonic chip.

V. CONCLUSION

In conclusion, we demonstrate a strongly coupled QD-cavity system integrated on a CMOS-processed silicon waveguide. The device is fabricated by the transfer-printing method, which overcomes the difficulty of the hybrid integration method. Low-temperature microphotoluminescence spectroscopy verifies the strong coupling between the QD and the cavity with observation of the vacuum Rabi splitting as well as the waveguide coupling of the cavity. This work serves as an important stepping stone toward the realization of novel quantum devices incorporating single-photon nonlinearity to be developed on the CMOS platform.

ACKNOWLEDGMENTS

We are grateful to K. Kuruma for fruitful discussion. This work was supported by the JSPS KAKENHI Grant-in-Aid for Specially Promoted Research (Grant No. 15H05700), KAKENHI Grant No. 16K06294, and the New Energy and Industrial Technology Development Organization (NEDO).

[1] J. L. O'Brien, A. Furusawa, and J. Vuckovic, Photonic quantum technologies, Nat. Photonics **3**, 687 (2009).
[2] J. W. Silverstone, D. Bonneau, J. L. O'Brien, and M. G. Thompson, Silicon quantum photonics, IEEE J. Sel. Top. Quantum Electron. **22**, 6700113 (2016).
[3] M. A. Nielsen and I. L. Chuang, *Quantum Computation and Quantum Information* (Cambridge University Press, Cambridge, 2010).
[4] I. M. Georgescu, S. Ashhab, and F. Nori, Quantum simulation, Rev. Mod. Phys. **86**, 153 (2014).
[5] N. Gisin, G. Ribordy, W. Tittel, and H. Zbinden, Quantum cryptography, Rev. Mod. Phys. **74**, 145 (2002).
[6] C. L. Degen, F. Reinhard, and P. Cappellaro, Quantum sensing, Rev. Mod. Phys. **89**, 035002 (2017).
[7] R. Soref, The past, present, and future of silicon photonics, IEEE J. Sel. Top. Quantum Electron. **12**, 1678 (2006).
[8] D. Dai, J. Bauters, and J. E. Bowers, Passive technologies for future large-scale photonic integrated circuits on silicon: Polarization handling, light non-reciprocity and loss reduction, Light: Sci. Appl. **1**, e1 (2012).
[9] J. M. Raimond, M. Brune, and S. Haroche, Manipulating quantum entanglement with atoms and photons in a cavity, Rev. Mod. Phys. **73**, 565 (2001).
[10] T. Aoki, B. Dayan, E. Wilcut, W. P. Bowen, A. S. Parkins, T. J. Kippenberg, K. J. Vahala, and H. J. Kimble, Observation of strong coupling between one atom and a monolithic microresonator, Nature **443**, 671 (2006).
[11] M. Steiner, H. M. Meyer, C. Deutsch, J. Reichel, and M. Köhl, Single Ion Coupled to an Optical Fiber Cavity, Phys. Rev. Lett. **110**, 043003 (2013).
[12] Y.-S. Park, A. K. Cook, and H. Wang, Cavity QED with diamond nanocrystals and silica microspheres, Nano Lett. **6**, 2075 (2006).
[13] Z.-L. Xiang, S. Ashhab, J. Q. You, and F. Nori, Hybrid quantum circuits: Superconducting circuits interacting with other quantum systems, Rev. Mod. Phys. **85**, 623 (2013).
[14] T. Yoshie, A. Scherer, J. Hendrickson, G. Khitrova, H. Gibbs, G. Rupper, C. Ell, O. Shchekin, and D. Deppe, Vacuum Rabi splitting with a single quantum dot in a photonic crystal nanocavity, Nature **432**, 200 (2004).
[15] J. P. Reithmaier, G. Sek, A. Löffler, C. Hofmann, S. Kuhn, S. Reitzenstein, L. V. Keldysh, V. D. Kulakovskii, T. L. Reinecke, and A. Forchel, Strong coupling in a single quantum dot-semiconductor microcavity system, Nature **432**, 197 (2004).
[16] X. Mi, J. V. Cady, D. M. Zajac, P. W. Deelman, and J. R. Petta, Strong coupling of a single electron in silicon to a microwave photon, Science **355**, 156 (2017).
[17] P. Michler, A. Kiraz, C. Becher, W. V. Schoenfeld, P. M. Petreff, L. Zhang, E. Hu, and A. Imamoglu, A quantum dot single-photon turnstile device, Science **290**, 2282 (2000).
[18] A. Kuhn, M. Hennrich, and G. Rempe, Deterministic Single-Photon Source for Distributed Quantum Networking, Phys. Rev. Lett. **89**, 067901 (2002).
[19] D. Englund, B. Shields, K. Rivoire, F. Hatami, J. Vuckovic, H. Park, and M. D. Lukin, Deterministic coupling of a single nitrogen vacancy center to a photonic crystal cavity, Nano Lett. **10**, 3922 (2010).
[20] A. A. Houck, D. I. Schuster, J. M. Gambetta, J. A. Schreier, B. R. Johnson, J. M. Chow, L. Frunzio, J. Majer, M. H. Devoret, S. M. Girvin, and R. J. Shoelkopf, Generating single microwave photons in a circuit, Nature **449**, 328 (2007).
[21] I. Shomroni, S. Rosenblum, Y. Lovsky, O. Bechler, G. Guendelman, and B. Dayan, All-optical routing of single photons by a one-atom switch controlled by a single photon, Science **345**, 903 (2014).
[22] T. Volz, A. Reinhard, M. Winger, A. Badolato, K. J. Hennessy, E. L. Hu, and A. Imamoglu, Ultrafast all-optical switching by single photons, Nat. Photonics **6**, 605 (2012).

[23] T.-C. Hoi, C. M. Wilson, G. Johansson, T. Palomaki, B. Peropadre, and P. Delsing, Demonstration of a Single-Photon Router in the Microwave Regime, Phys. Rev. Lett. **107**, 073601 (2011).

[24] T. G. Tiecke, J. D. Thompson, N. P. de Leon, L. R. Liu, V. Vuletic, and M. D. Lukin, Nanophotonic quantum phase switch with a single atom, Nature **508**, 241 (2014).

[25] A. Javadi, I. Söllner, M. Arcari, S. Lindskov Hansen, L. Midolo, S. Mahmoodian, G. Kirsanske, T. Pregnolato, E. H. Lee, J. D. Song, S. Stobbe, and P. Lodahl, Single-photon non-linear optics with a quantum dot in a waveguide, Nat. Commun. **6**, 8655 (2015).

[26] I. E. Zadeh, A. W. Elshaari, K. D. Jöns, A. Fognini, D. Dalacu, P. J. Poole, M. E. Reimer, and V. Zwiller, Deterministic integration of single photon sources in silicon based photonic circuits, Nano Lett. **16**, 2289 (2016).

[27] A. W. Elshaari, I. E. Zadeh, A. Fognini, M. E. Reimer, D. Dalacu, P. J. Poole, V. Zwiller, and K. D. Jöns, On-chip single photon filtering and multiplexing in hybrid quantum photonic circuits, Nat. Commun. **8**, 379 (2017).

[28] J.-H. Kim, S. Aghaeimeibodi, C. J. K. Richardson, R. P. Leavitt, D. Englund, and E. Waks, Hybrid integration of solid-state quantum emitters on a silicon photonic chip, Nano Lett. **17**, 7394 (2017).

[29] M. Davanco, J. Liu, L. Sapienza, C.-Z. Zhang, J. V. De Miranda Cardoso, V. Verma, R. Mirin, S. W. Nam, L. Liu, and K. Srinivasan, Heterogeneous integration for on-chip quantum photonic circuits with single quantum dot devices, Nat. Commun. **8**, 889 (2017).

[30] I. J. Luxmoore, R. Toro, O. Del Pozo-Zamudio, N. A. Wasley, E. A. Chekhovich, A. M. Sanchez, R. Beanland, A. M. Fox, M. S. Skolnick, H. Y. Liu, and A. I. Tartakovskii, III-V quantum light source and cavity-QED on silicon, Sci. Rep. **3**, 1239 (2013).

[31] E. Menard, K. J. Lee, D.-Y. Khang, R. G. Nuzzo, and J. A. Rogers, A printable form of silicon for high performance thin film transistors on plastic substrates, Appl. Phys. Lett. **84**, 5398 (2004).

[32] M. A. Meitl, Z.-T. Zhu, V. Kumar, K. J. Lee, X. Feng, Y. Y. Huang, I. Adesida, R. G. Nuzzo, and J. A. Rogers, Transfer printing by kinetic control of adhesion to an elastomeric stamp, Nat. Mater. **5**, 33 (2006).

[33] J. Yoon, S.-M. Lee, D. Kang, M. A. Meitl, C. A. Bower, and J. A. Rogers, Heterogeneously integrated optoelectronic devices enabled by micro-transfer printing, Adv. Optical Mater. **3**, 1313 (2015).

[34] M. Brune, S. Haroche, V. Lefevre, J. M. Raimond, and N. Zagury, Quantum Nondemolition Measurement of Small Photon Numbers by Rydberg-Atom Phase-Sensitive Detection, Phys. Rev. Lett. **65**, 976 (1990).

[35] A. Wallraff, D. I. Schuster, A. Blais, L. Frunzio, R.-S. Huang, J. Majer, S. M. Girvin, and R. J. Schoelkopf, Strong coupling of a single photon to a superconducting qubit using circuit quantum electrodynamics, Nature **431**, 162 (2004).

[36] P. B. Deotare, M. W. McCutcheon, I. W. Frank, M. Khan, and M. Loncar, High quality factor photonic crystal nanobeam cavities, Appl. Phys. Lett. **94**, 121106 (2009).

[37] E. Kuramochi, H. Taniyama, T. Tanabe, K. Kawasaki, Y.-G. Roh, and M. Notomi, Ultrahigh-Q one-dimensional photonic crystal nanocavities with modulated mode-gap barriers on SiO_2 claddings and on air claddings, Opt. Express **18**, 15859 (2010).

[38] Y. Gong, B. Ellis, G. Shambat, T. Sarmiento, J. S. Harris, and J. Vuckovic, Nanobeam photonic crystal cavity quantum dot laser, Opt. Express **18**, 8781 (2010).

[39] R. Ohta, Y. Ota, M. Nomura, N. Kumagai, S. Ishida, S. Iwamoto, and Y. Arakawa, Strong coupling between a photonic crystal nanobeam cavity and a single quantum dot, Appl. Phys. Lett. **98**, 173104 (2011).

[40] R. Katsumi, Y. Ota, M. Kakuda, S. Iwamoto, and Y. Arakawa, Transfer-printed single-photon sources coupled to wire waveguides, Optica **5**, 691 (2018).

[41] A. Osada, Y. Ota, R. Katsumi, K. Watanabe, S. Iwamoto, and Y. Arakawa, Transfer-printed quantum-dot nanolasers on a silicon photonic circuit, Appl. Phys. Express **11**, 072002 (2018).

[42] K. Hennessy, A. Badolato, M. Winger, D. Gerace, M. Atatüre, S. Gulde, S. Fält, E. L. Hu, and A. Imamoglu, Quantum nature of a strongly coupled single quantum dot-cavity system, Nature **445**, 896 (2007).

[43] K. Kuruma, Y. Ota, M. Kakuda, S. Iwamoto, and Y. Arakawa, Time-resolved vacuum Rabi oscillations in a quantum-dot-nanocavity system, Phys. Rev. B **97**, 235448 (2018).

[44] E. T. Jaynes and F. W. Cummings, Comparison of quantum and semiclassical radiation theories with application to the beam maser, Proc. IEEE **51**, 89 (1963).

[45] K. Kuruma, Y. Ota, M. Kakuda, D. Takamiya, S. Iwamoto, and Y. Arakawa, Position dependent optical coupling between single quantum dots and photonic crystal nanocavities, Appl. Phys. Lett. **109**, 071110 (2016).